NUCL SCI TECH (2018) 29:12
https://doi.org/10.1007/s41365-017-0352-2

Effect of H_2 dilution on the structure and properties of nc-CrC/a-C:H coatings deposited by a hybrid beams system

Yao Cai[1] · Hui-Dong Liu[1] · Zhong-Wei Hu[2] · Qiang Wan[1] · Chang Luo[3] · Hao Chen[1] · Yan Liu[1] · Yan-Ming Chen[1] · Qing-Song Mei[1] · Bing Yang[1]

Received: 10 October 2016 / Revised: 8 March 2017 / Accepted: 19 March 2017 / Published online: 29 December 2017

Abstract Nanocomposite CrC/hydrogenated amorphous carbon (nc-CrC/a-C:H) coatings were deposited by a hybrid beams system comprised of a hollow cathode ion source and a cathodic arc ion-plating unit with varying H_2 flow rates. The influences of H_2 flow rates on the morphologies, microstructures, and properties of the coatings were systematically studied. The morphologies and microstructures of the coatings were characterized by SEM, AFM, XPS, Raman spectroscopy, GIXRD, and HRTEM. The mechanical and tribological properties were measured by a nano-indenter, scratch tester, and ball-on-disk tribometer. The wear tracks were evaluated using 3D profilometer, optical microscope, and EDS analysis. It has been found that a moderate H_2 flow rate can effectively smooth the surface, enlarge the fraction of a sp^3 bond, and improve the properties. The coating exhibits the highest hardness and elastic modulus at the H_2 flow rate of 40 sccm. A superior combination of adhesion strength, friction coefficient, and wear resistance can be achieved at the H_2 flow rate of 80 sccm.

Keywords CrC/a-C:H coating · Nanocomposite · H_2 flow rate · Hybrid beams system

This work was supported by the National Natural Science Foundation of China (Nos. 11275141 and 11175133), the International Cooperation Program of the Ministry of Science and Technology of China (No. 2015DFR00720), the Center for Electron Microscopy of Wuhan University, the Center of Nanosci. and Nanotech, Research of Wuhan University, and the Analysis and Test Center of Wuhan University.

✉ Bing Yang
toyangbing@whu.edu.cn

[1] School of Power and Mechanical Engineering, Wuhan University, Wuhan 430072, China

[2] School of Materials Science and Engineering, Xi'an Jiao Tong University, Xi'an 710049, China

[3] China Datang Corporation Science and Technology Research Institute Co. Ltd., East China Branch, Hefei 230000, China

1 Introduction

Nanocomposite coatings consisting of an amorphous hydrogenated carbon (a-C:H or diamond-like carbon, DLC) matrix and hard crystalline carbides have attracted considerable attention in both industrial application and the research field owing to their excellent mechanical and tribological performances [1–3]. Numerous works have been devoted to synthesize the nanocomposite coatings by introducing carbide forming metals (Cr [4, 5], Ti [6], Cu [7], and W [8, 9]) into an a-C:H phase to overcome some shortcomings of DLC coatings, such as high internal stress, poor thermal stability, and low adhesion to substrates. Herein, metallic Cr as a carbide former plays a positive role in reducing stress and strengthening adhesion of the coating while maintaining the outstanding corrosion resistance, hardness, and friction coefficient of DLC coatings [5, 10, 11]. Gassner et al. [12] processed a detailed research about the structure–property relationship in CrC/a-C:H coatings synthesized by a reactive magnetron sputtering. Singh et al. [5] systematically investigated the characterization and properties of CrC/a-C:H coatings synthesized by a hybrid PVD/PECVD deposition and found that the Cr content has a significant influence on the microstructure and tribological properties of CrC/a-C:H coatings. Liu et al. [13] used Cr adulterant to enhance the performances of DLC coatings and successfully fabricated a hydrogenated Cr/a-C coating with a high nano-hardness of 15.7 GPa and good adhesion strength with a critical load of 36 N.

For the nanocomposite CrC/a-C:H (nc-CrC/a-C:H) coatings, the structure and properties are strongly dependent upon the formation of carbides, amorphous structures of sp^2 and sp^3 bonds, which are significantly correlated with the process conditions. Previous experiments have shown that the presence of hydrogen is an important factor for the good properties of DLC coatings [3, 14]. Casiraghi et al. [15] have systematically studied the influence of hydrogen content on a-C:H coatings by Raman spectroscopy and found that the hydrogen is tightly correlated with the configuration and amount of sp^2 and sp^3 phases, thus affecting the mechanical and optical performances of coatings. Furthermore, the hydrogen dilution can also influence the tribological properties, thermal stability, adhesion strength, and graphitization of DLC coatings [14, 16–20]. However, among the literatures related to the role of hydrogen on DLC coatings, most of them are devoted studying the effect of hydrogen on the unmixed DLC or a-C:H coating. The nature of nc-CrC/a-C:H coatings has a complex relationship with the hydrogen dilution due to the doped chromium carbides, though few researches have processed a comprehensive study about the effects of hydrogen on the microstructure and properties of nc-CrC/a-C:H coatings.

In this work, nc-CrC/a-C:H coatings were synthesized by a hybrid beams system comprised of a hollow cathode ion source (HCIS) and a cathodic arc ion-plating unit. The effects of hydrogen dilution on the morphologies, microstructures, and properties of coatings were studied in detail.

2 Experimental details

2.1 Coatings deposition

Figure 1 shows the homemade direct current hybrid beams system used in this study, which is equipped with two Cr targets (purity, 99.99%) and one HCIS on the chamber wall. Both of the Cr targets and the HCIS face the substrates at an angle of 45°. The distance between the targets (or HCIS) and the substrates is approximately 20 cm.

The nc-CrC/a-C:H coatings were synthesized on tungsten carbides, stainless steel (austenitic 304), and silicon (100) wafers substrates at C_2H_2, H_2, and Ar ambient under various H_2 flow rates. All the substrates were cleaned in acetone by the ultrasonic for 10 min, rinsed by deionized water, and dried in a constant temperature cabinet of 60 °C. Then the substrates were placed sideways on a rotating

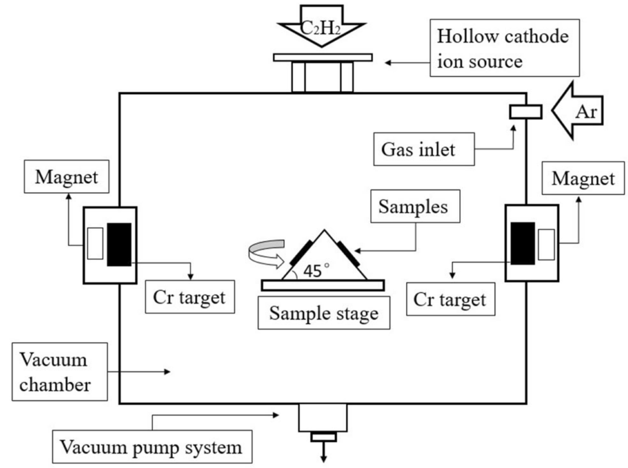

Fig. 1 Schematic diagram of the hybrid beams system

sample holder, which is located in the center of the chamber. Before the coating deposition, the experimental chamber was pumped down to the pressure of 7×10^{-3} Pa and the chamber ambient was heated up to 250 °C by an accessional heater. The temperature of the experimental chamber was constantly monitored by a thermocouple located in the top center of the chamber. A high direct current bias voltage of − 900 V was applied to the experimental substrates and the Cr target current was set as 80 A to offer high-energy ions to clean the substrates. The deposition conditions of coatings are shown in Table 1. The C_2H_2 and H_2 gases were introduced through the HCIS and ionized by the HCIS plasma. For all coating deposition processes, the substrates rotation speed was set at 4 rpm and the value of accessional heater was maintained at 250 °C, while the pressure of the chamber was kept at 0.5 Pa by controlling the Ar flow rate. The H_2 flow rates

Table 1 Detailed deposition conditions of the nc-CrC/a-C:H coatings

Parameters	Value
Target material (Cr)	99.99%
Bias voltage (V)	− 150, 80% duty cycle
Reactive gas	C_2H_2, H_2
Working pressure (Pa)	0.5
C_2H_2 flow rate (sccm)	150
Cr target current (A)	50
HCIS current (A)	60
Heater temperature (°C)	250
Rotation speed (rpm)	4
Deposition time (min)	60
H_2 flow rate (sccm)	20, 40, 80, 120, 150

were different for each deposition: 20, 40, 80, 120, and 150 sccm.

2.2 Characterization of coatings

The surface and cross-sectional morphologies of coatings were observed by a scanning electron microscopy (SEM, FEI Sirion IMP). The surface topographies were probed by an atomic force microscopy (AFM, Shimadzu SPM-9500J3) employed in the tapping mode with a measuring area of 5 × 5 um^2. The chemical bonding states were investigated using an X-ray photoelectron spectroscopy (XPS, ESCALAB 250Xi) using Al K_α (1486.6 eV) X-ray radiation. A laser confocal Raman microspectroscopy (Renishaw RM 1000) with Ar+ laser excitation (514.5 nm) was used to determine the content of the sp^3 hybrid bond and G, D peak position. The microstructure was analyzed by a high-resolution transmission electron microscope (HRTEM, JEM-2100 HR) operated at 200 kV and a grazing incidence X-ray diffraction (GIXRD, D8 ADVANCE, and DAVINCI DESIGN) performed on an X-ray diffractometer with a Cu K_α radiation (0.154 nm) at a grazing incidence angle of 3°.

The hardness and elastic modulus were measured with a nano-indenter (MT-G200) equipped with a Berkovich diamond tip. The indenter load increased at constant displacement rate, until a depth of 100 nm was achieved. This maximum indentation penetration depth was only less than 1/10th of the coating thickness to minimize the influence of substrate on the measure results [21]. Furthermore, the scratch tests were operated by a HH-3000 tester in a continuous load of 0–50 N. The loading rate and moving speed were kept at 50 N/min and 4 mm/min, respectively. The tribological performance was evaluated at room temperature in ambient air (23 °C, relative humidity of 30%) during dry sliding experiments conducted with a conventional ball-on-disk wear tester (MS-T3000). Here, the Si_3N_4 ball (99.9%, purity) with the diameter of 3 mm was used as mated materials, and 2–3 measurements were made for each sample. A load of 500 gf and a sliding speed of 100 rounds per minute for 30 min were carried out. The radius of the friction trajectory was set as 3 mm. The images and corresponding chemical composition of wear tracks were investigated by an optical microscope (Zeiss Axio Lab. A1) and a EDAX genesis 7000 EDS, respectively. The wear rates of coatings were calculated by measuring the wear tracks using a 3D optical profilometer (Contour GT-K, Bruker).

3 Results and discussions

3.1 Surface and cross-sectional morphologies

Figure 2 displays the surface images of the as-deposited coatings synthesized at varying H_2 flow rates. The surfaces of the coatings contain obvious micro-droplets, which are characteristic of cathodic arc ion-plating. As the H_2 flow rate varies in the range of 20–150 sccm, the coating synthesized at the H_2 flow rate of 80 sccm exhibits the smoothest surface morphology with low distribution density and small size of micro-droplets, which can be attributed to the appropriate level of hydrogen ions etching [22]. The 3D AFM morphologies of the coatings are given in Fig. 3, and the variation of surface roughness measured by AFM is shown in Fig. 4. It is noted that the square average roughness (R_{ms}) reduces from 63.8 to 16.7 nm and the arithmetic mean roughness (R_a) decreases from 48 to 13.2 nm when H_2 flow rate increases from 20 to 80 sccm. The R_{ms} and R_a of the as-deposited coatings showed a gradient increase with further H_2 flow rate. The result is consistent with the SEM ones. It can be considered that the optimal H_2 flow rate smooths the surface, but the surface roughness increases drastically with a large or less degree of H_2 flow rate. The representative cross-sectional image of the coating deposited at the H_2 flow rate of 40 sccm is displayed in Fig. 5, in which the coating exhibits a very dense structure and homogeneous morphology. In particular, the thickness of the nc-CrC/a-C:H coatings decreases from 1.88 to 1.38 um as the H_2 flow rate increases from 20 to 150 sccm.

3.2 Microstructure

Figure 6 exhibits the XPS C 1s and Cr 2p spectra of the coating synthesized at the H_2 flow rate of 80 sccm. As seen in Fig. 6a, the analysis of the C 1s spectra was operated by resolving into five Gaussian peaks. The two peaks at the binding energy around 284.2 and 284.7 eV correspond to sp^2-C and sp^3-C bonding, which confirms the presence of amorphous carbon phase in coatings [4]. The peak at 283.2 eV corresponds to the carbon phase in chromium carbide, and the carbon peaks at 286.4 and 288.6 eV can be attributed to adsorbed oxygen [23, 24]. The Cr $2p^{3/2}$ spectra were fitted into three peaks ascribed to Cr–C (574.4 eV), Cr–O (Cr^{6+}, 575.2 eV), and Cr–O (Cr^{3+}, 576.7 eV) bonding states [25, 26].

In addition to the XPS analysis, Raman spectroscopy can promote a result of the more accurate data and in-depth research on account of the sensitivity of this tool to the diversified structures of carbon. As shown in Fig. 7a, the presence of amorphous carbon in our coatings is definitely

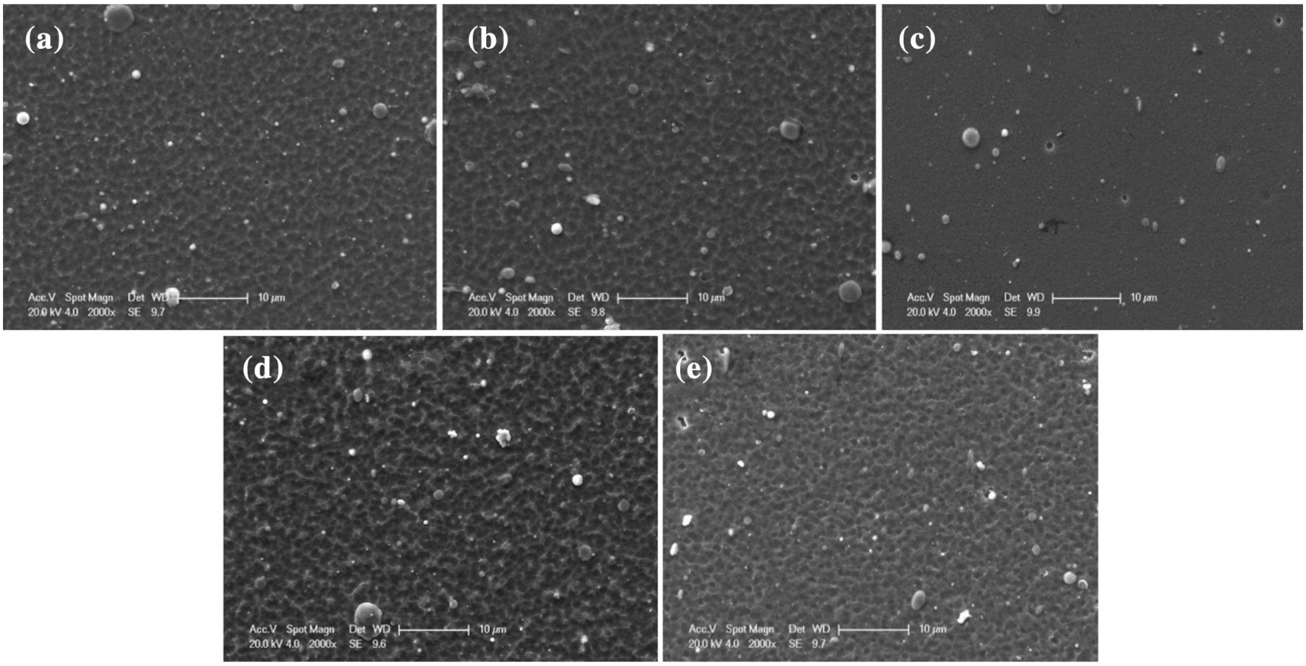

Fig. 2 Surface SEM images of the coatings. **a** 20 sccm, **b** 40 sccm, **c** 80 sccm, **d** 120 sccm, and **e** 150 sccm

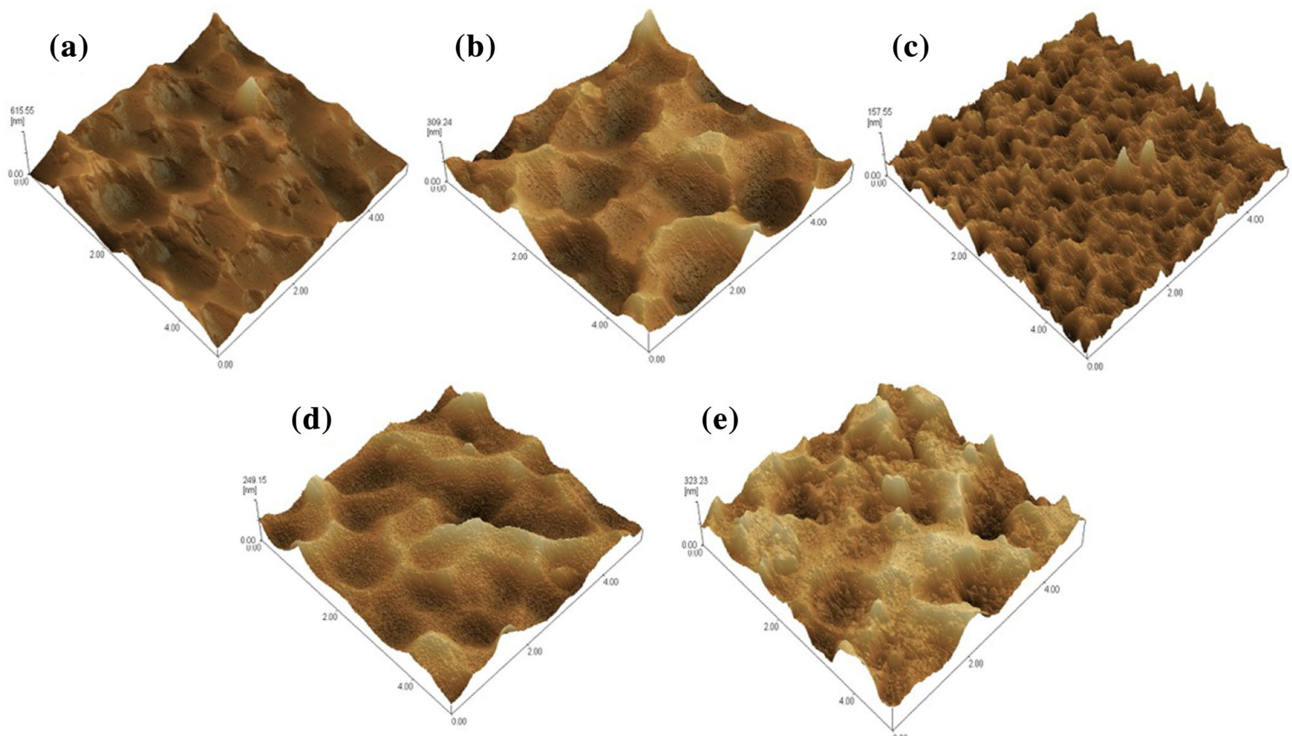

Fig. 3 (Color online) AFM images of the as-deposited coatings synthesized at different H_2 flow rates: **a** 20 sccm, **b** 40 sccm, **c** 80 sccm, **d** 120 sccm, and **e** 150 sccm

confirmed by the Raman spectroscopy result, which exhibits the characteristic peaks (D and G peaks) of a-C:H coatings [27]. In order to perform a more detailed analysis, Raman spectra of the coatings were deconvoluted into four peaks (D1, D2, G1, and G2 peaks) using Gaussian function to calculate the peak positions and the ratio of peak areas [$I_D/I_G = I(\mathrm{D1} + \mathrm{D2})/I(\mathrm{G1} + \mathrm{G2})$] presented in the different as-deposited coatings [12, 24]. Figure 7b presents

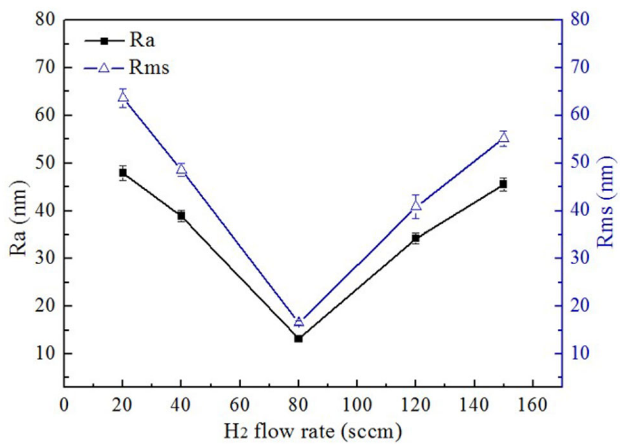

Fig. 4 R_{ms} and R_a of the coatings as a function of H_2 flow rates

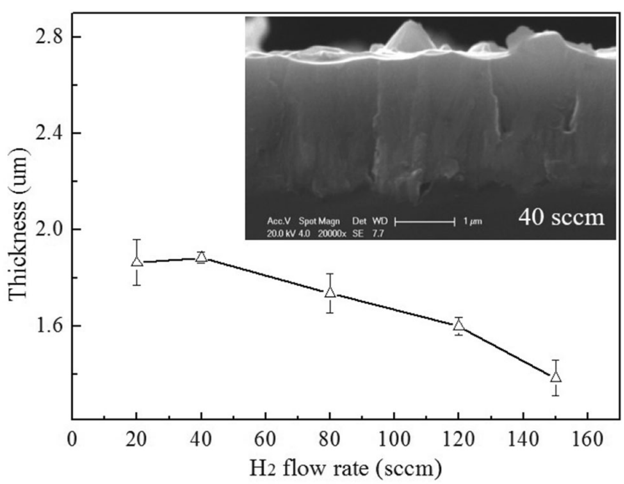

Fig. 5 Coating thickness with the representative cross-sectional SEM image

the curves-fitted Raman spectroscopy data. The sp^3/sp^2 ratio can be characterized by the I_D/I_G ratio, and the increasing sp^3 fraction in the amorphous carbon coatings will decrease the I_D/I_G ratio [28, 29]. As the H_2 flow rate increases from 20 to 80 sccm, the I_D/I_G decreases continuously from 1.16 to 0.92 with the simultaneous decrease in the G1 peak position. With further H_2 flow rate, both of the I_D/I_G and G1 peak positions tend to increase. The Raman spectroscopy result shows that an optimal H_2 flow rate leads to an increasing formation of a sp^3 phase and generates a transitional formation from the graphite-like carbon to the amorphous carbon in the a-C:H coatings [30].

The GIXRD diffractions measured in stainless steel samples reveal the structural evolution in the nc-CrC/a-C:H coatings, and the results are displayed in Fig. 8. For all coatings, the diffraction peaks can be assigned to Cr_3C_2 phases via referring to the JCPDS database card no. 35-0804 [12, 13]. In particular, the signals of chromium carbide phases become feeble as the H_2 flow rate increases from 40 to 150 sccm, indicating that increased hydrogen dilution suppresses the formation of chromium carbide nanocrystals. For a more in-depth understanding of the microstructure, the cross-sectional HRTEM of the coating synthesized on a Si substrate at the H_2 flow rate of 80 sccm has been completed. The nanocomposite structure consisting of the uniform nanocrystals and amorphous carbon matrix can be clearly observed in Fig. 9, in which the sizes of nanocrystals are about 4–6 nm. Furthermore, the nanocrystalline phases can be identified as Cr_3C_2 phases by the corresponding SAED pattern where four major reflections can be observed.

3.3 Mechanical and tribological properties

Mechanical performance of the as-deposited coatings intrinsically depends on the bonding states and chromium carbide phases. A higher ratio of sp^3/sp^2, optimal chromium carbides structure can preferentially form a three-dimensional, interconnected structure to increase the hardness and elastic modulus of coatings [3]. Figure 10

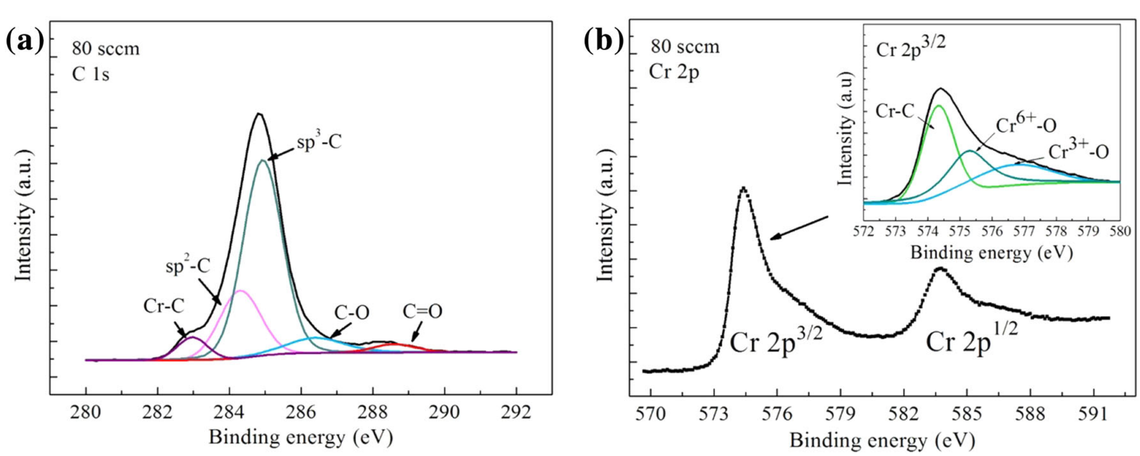

Fig. 6 (Color online) Gaussian fitting of **a** C 1s and **b** Cr 2p for the coatings deposited at the H_2 flow rate of 80 sccm

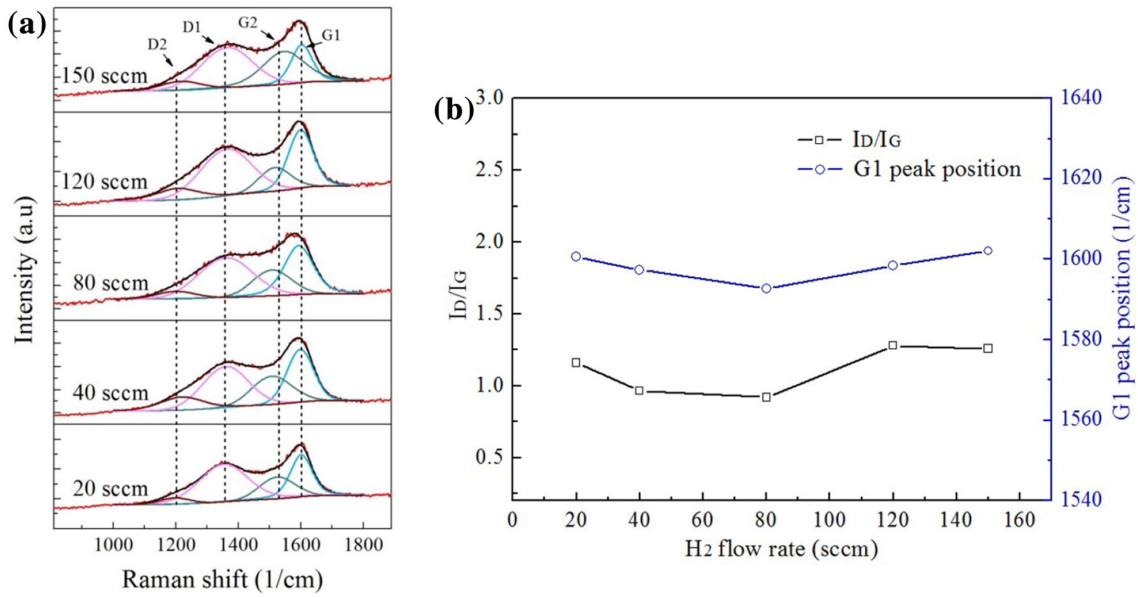

Fig. 7 (Color online) **a** Raman spectra and **b** I_D/I_G ratio and G1 peak position of the coatings

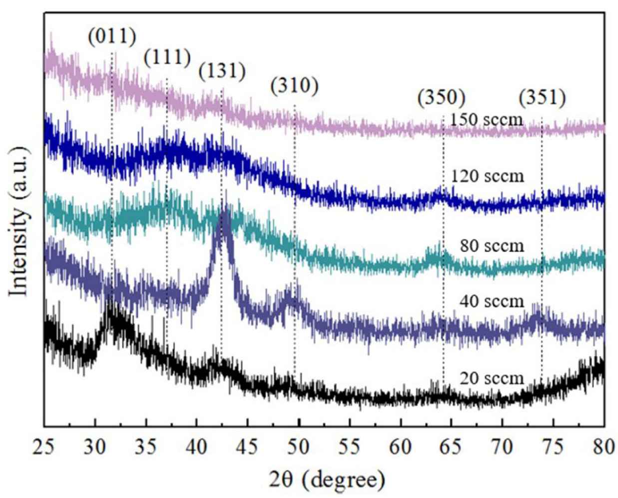

Fig. 8 (Color online) GIXRD patterns of the coatings

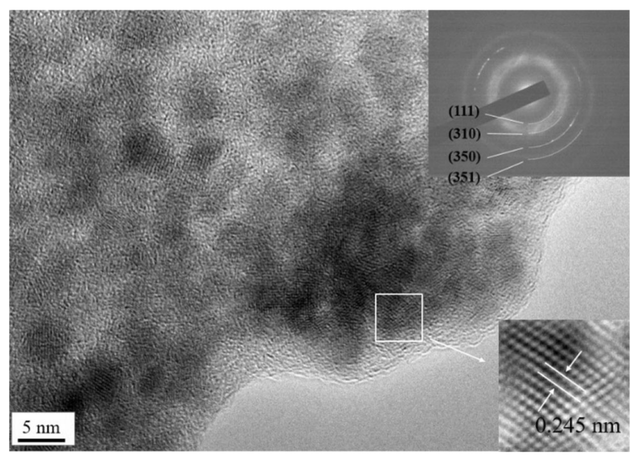

Fig. 9 Cross-sectional HRTEM image of the coating deposited at the H_2 flow rate of 80 sccm

exhibits the variation of the hardness and elastic modulus as a function of H_2 flow rate. It is noted that the coating deposited at the H_2 flow rate of 40 sccm has the highest hardness and elastic modulus of 28.1 and 534.2 GPa, respectively, while the coating synthesized at the H_2 flow rate of 150 sccm owns the lowest hardness as well as elastic modulus of only 19.1 and 378.5 GPa, respectively. The variation of hardness and elastic modulus can be attributed to the comprehensive influence between sp^3 carbon and chromium carbide nanocrystals. In particular, the suppressed formation of hard nanocrystals is possibly the dominant reason for the decrease on hardness and elastic modulus, since the decreased chromium carbide

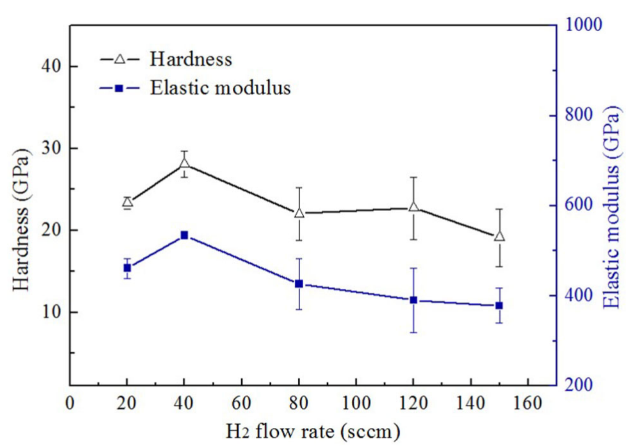

Fig. 10 Hardness and friction coefficient of the coatings

nanocrystals cause less interfaces or increscent mean grain separation [31].

The scratch tests of the as-deposited coatings on the cemented carbide substrates were operated to characterize the critical load. In the adhesion test, damage and cracks first appeared and progressed in the amorphous phase, which led to the coating spallation and exposed the base material, thus causing an increasing friction coefficient [32]. The critical loading (L_C) was measured by the acoustic emission signal and the inflection point in the frictional force curves. The load at which the first crack occurred was referred to the lower critical load L_{C1} and the load corresponding to coating delamination was called the higher critical load L_{C2} [33]. As shown in Fig. 11, the coating shows the maximal critical load, L_{C1}, of 12.5 N and L_{C2} of 21 N at the H_2 flow rate of 80 sccm. Actually, during the indenter sliding, the adhesion failures are significantly influenced by the shear stresses occurring in the interface induced by the normal applied load and the tangential load generated. The increased H_2 dilution leads to a significant reduction of the compression residual stress that will retard the failure occurrence, thus giving a rise to the critical load, L_C [34]. However, the adhesion strength is lower for the higher H_2 flow rate and, in this work, that can be attributed to the decrease of coating thickness [35].

The influence of H_2 flow rate on the friction and wear performances of the as-deposited coatings was examined by a ball-on-disk tribometer. Figure 12 displays the friction coefficient and wear rate of the coatings. It is clearly seen that the friction coefficient of coatings shows a decreasing tendency followed by a subsequent increase as the H_2 flow rate increases from 20 to 150 sccm and minimizes at 80 sccm at about 0.16. Meanwhile, the specific wear rate Ws exhibits the smallest value of 4.17×10^{-6} mm^3/N m

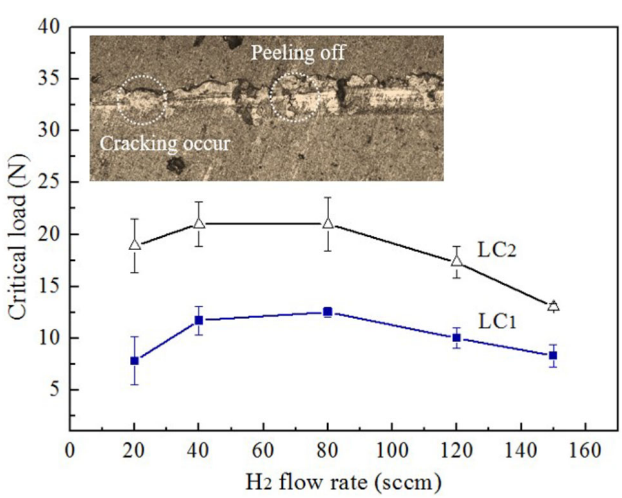

Fig. 11 (Color online) Critical loads of scratch test with the inserted optical microscope image of coating failure in the scratch test

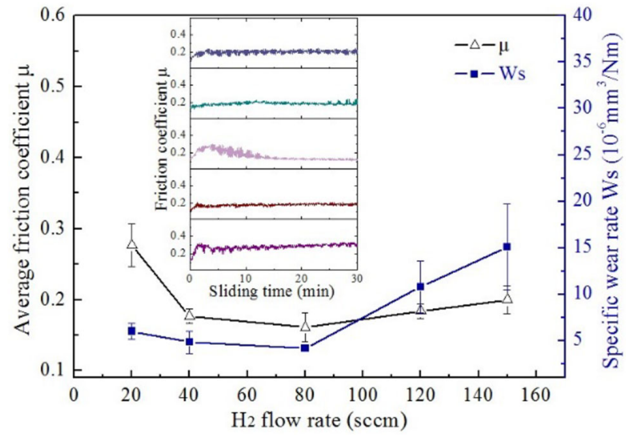

Fig. 12 Friction curves of the coatings sliding against Si_3N_4 balls in ambient air

when the H_2 flow rate reaches 80 sccm. The variations of friction coefficient and wear rate can be due to the hydrogen dilution significantly affecting the tribological performances by dominating the sp^3/sp^2 ratio, or the roughness [36]. The measured wear tracks with EDS analysis are displayed in Fig. 13, which presents the tribological performance of the coatings. For the EDS analysis, the change of chemical content along with the axial direction of wear tracks agrees with the wear rate behavior. Furthermore, the wear microgrooves observed on the wear tracks are most likely caused by trapped wear debris particles during sliding motion. A notable smooth surface is exhibited on the wear track displayed in Fig. 13c, which suggests the degree of abrasive wear becomes less dominant and the asperities are polished.

4 Conclusion

The nc-CrC/a-C:H coatings are synthesized using a hybrid beams system, which consists of a HCIS and a cathodic arc ion-plating unit. The effect of H_2 flow rate on the microstructures, morphologies, and mechanical properties is studied systematically. The surface morphologies show a significant change in surface structures with the variation of H_2 flow rate and confirm that an optimal H_2 dilution can effectively smooth the surface due to the hydrogen etching. The microstructure analysis allows us to conclude that increased H_2 flow rate trends to impede the formation of chromium carbide nanocrystals and the H_2 flow rate of 80 sccm corresponds to the maximal sp^3/sp^2. The highest hardness and elastic modulus of 28.1 and 534.2 GPa, respectively, can be obtained at the H_2 flow rate of 40 sccm. Under a H_2 flow rate of 80 sccm, the coating can achieve a combination of good adhesion strength (critical load L_{C1} of 12.5 N and L_{C2} of 21 N), low

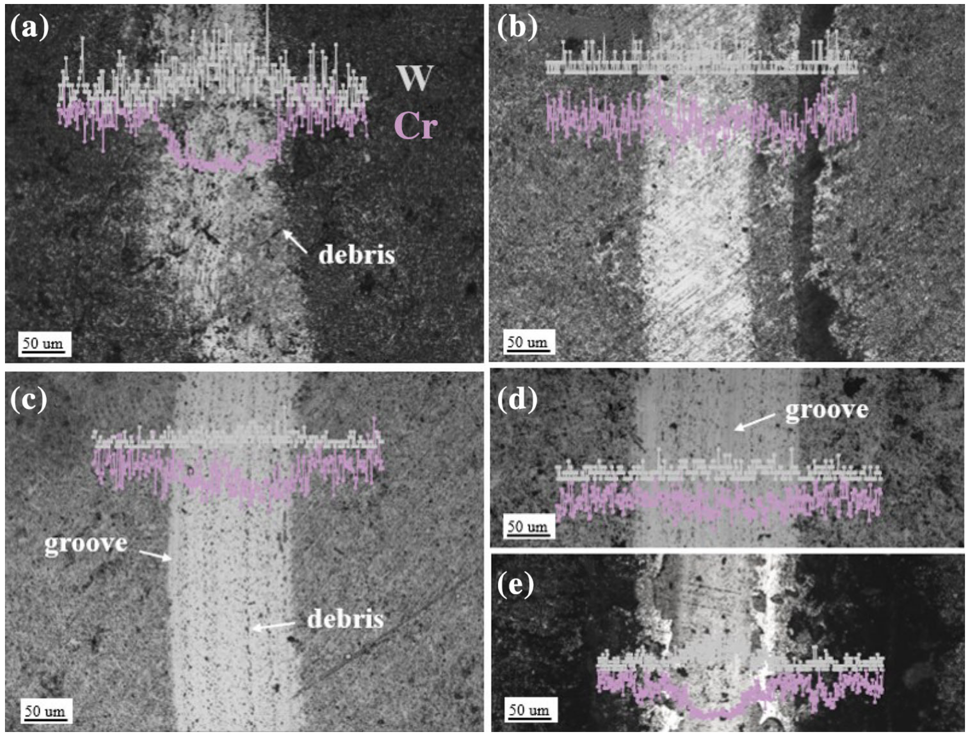

Fig. 13 (Color online) Optical images with corresponding EDS analysis of wear tracks. **a** 20 sccm, **b** 40 sccm, **c** 80 sccm, **d** 120 sccm, **e** 150 sccm

friction coefficient (0.16), and excellent wear resistance (4.17×10^{-6} mm^3/N m).

References

1. S.J. Bull, Tribology of carbon coatings: DLC, diamond and beyond. Diam. Relat. Mater. **4**, 827–836 (1995). https://doi.org/10.1016/0925-9635(94)05325-1
2. R. Gilmore, R. Hauert, Control of the tribological moisture sensitivity of diamond-like carbon films by alloying with F, Ti or Si. Thin Solid Films **398**, 199–204 (2001). https://doi.org/10.1016/S0040-6090(01)01437-7
3. J. Robertson, Diamond-like amorphous carbon. Mater. Sci. Eng., R **37**, 129–281 (2002). https://doi.org/10.1016/S0927-796X(02)00005-0
4. W. Dai, P. Ke, A. Wang, Microstructure and property evolution of Cr-DLC films with different Cr content deposited by a hybrid beam technique. Vacuum **85**, 792–797 (2011). https://doi.org/10.1016/j.vacuum.2010.11.013
5. V. Singh, J.C. Jiang, E.I. Meletis, Cr-diamondlike carbon nanocomposite films: synthesis, characterization and properties. Thin Solid Films **489**, 150–158 (2005). https://doi.org/10.1016/j.tsf.2005.04.104
6. W.J. Meng, R.C. Tittsworth, L.E. Rehn, Mechanical properties and microstructure of TiC/amorphous hydrocarbon nanocomposite coatings. Thin Solid Films **377**, 222–232 (2000). https://doi.org/10.1016/S0040-6090(00)01300-6
7. P. Guo, L. Sun, X. Li et al., Structural properties and surface wettability of Cu-containing diamond-like carbon films prepared by a hybrid linear ion beam deposition technique. Thin Solid Films **584**, 289–293 (2015). https://doi.org/10.1016/j.tsf.2015.01.018
8. H. Miki, T. Takeno, T. Takagi, Tribological properties of multilayer DLC/W-DLC films on Si. Thin Solid Films **516**, 5414–5418 (2008). https://doi.org/10.1016/j.tsf.2007.07.113
9. Y.T. Pei, X.L. Bui, X.B. Zhou et al., Tribological behavior of W-DLC coated rubber seals. Surf. Coat. Technol. **202**, 1869–1875 (2008). https://doi.org/10.1016/j.surfcoat.2007.08.013
10. C.W. Zou, H.J. Wang, L. Feng et al., Effects of Cr concentrations on the microstructure, hardness, and temperature-dependent tribological properties of Cr-DLC coatings. Appl. Surf. Sci. **286**, 137–141 (2013). https://doi.org/10.1016/j.apsusc.2013.09.036
11. S. Zhou, L. Wang, Z. Lu et al., Tailoring microstructure and phase segregation for low friction carbon-based nanocomposite coatings. J. Mater. Chem. **22**, 15782–15792 (2012). https://doi.org/10.1039/C2JM30918A
12. G. Gassner, P.H. Mayrhofer, C. Mitterer et al., Structure–property relations in Cr–C/a-C:H coatings deposited by reactive magnetron sputtering. Surf. Coat. Technol. **200**, 1147–1150 (2005). https://doi.org/10.1016/j.surfcoat.2005.02.186
13. L. Liu, S.G. Zhou, Z.B. Liu et al., Effect of chromium on structure and tribological properties of hydrogenated Cr/a-C:H films prepared via a reactive magnetron sputtering system, Chinese. Phys. Lett. **33**, 026801–026805 (2016). https://doi.org/10.1088/0256-307X/33/2/026801
14. X. Jiang, K. Reichelt, B. Stritzker, Mechanical properties of a-C:H films prepared by plasma decomposition of C_2H_2. J. Appl. Phys. **67**, 487–494 (1990). https://doi.org/10.1063/1.346738
15. C. Casiraghi, A.C. Ferrari, J. Robertson, Raman spectroscopy of hydrogenated amorphous carbons. Phys. Rev. B: Condens. Matter **72**, 085401 (2005). https://doi.org/10.1103/PhysRevB.72.085401
16. S. Neuville, A. Matthews, A perspective on the optimisation of hard carbon and related coatings for engineering applications. Thin Solid Films **515**, 6619–6653 (2007). https://doi.org/10.1016/j.tsf.2007.02.011
17. L. Cui, Z. Lu, L. Wang, Probing the low-friction mechanism of diamond-like carbon by varying of sliding velocity and vacuum

pressure. Carbon **66**, 259–266 (2014). https://doi.org/10.1016/j.carbon.2013.08.065
18. J. Robertson, Properties of diamond-like carbon. Surf. Coat. Technol. **50**, 185–203 (1992). https://doi.org/10.1016/0257-8972(92)90001-Q
19. S. Michaelson, A. Hoffman, Hydrogen bonding, content and thermal stability in nano-diamond films. Diamond Relat. Mater **15**, 486–497 (2006). https://doi.org/10.1016/j.diamond.2005.10.061
20. B.P. Swain, B.S. Swain, M.H. Nong, Effect of H2 dilution on a-CN:H films deposited by hot wire chemical vapour deposition. Appl. Surf. Sci. **255**, 9264–9267 (2009). https://doi.org/10.1016/j.apsusc.2009.07.020
21. Z. Han, J. Tian, J. Lao et al., Effects of thickness and substrate on the mechanical properties of hard coatings. J. Coat. Technol. Res. **1**, 337–341 (2004). https://doi.org/10.1007/s11998-004-0035-x
22. H. Kinoshita, M. Yamashita, T. Yamaguchi, Surface etching effects of amorphous C:H and CN_x:H films formed by super-magnetron plasma for field emission use. Thin Solid Films **516**, 3656–3660 (2008). https://doi.org/10.1016/j.tsf.2007.08.041
23. M. Tan, J. Zhu, J. Han et al., Relative fraction of sp^3 bonding in boron incorporated amorphous carbon films determined by X-ray photoelectron spectroscopy. Mater. Res. Bull. **43**, 1670–1678 (2008). https://doi.org/10.1016/j.materresbull.2007.07.033
24. L. Yate, L. Martínez-de-Olcoz, J. Esteve et al., Effect of the bias voltage on the structure of nc-CrC/a-C:H coatings with high carbon content. Surf. Coat. Technol. **206**, 2877–2883 (2012). https://doi.org/10.1016/j.surfcoat.2011.12.015
25. T.C. Kaspar, S.E. Chamberlin, M.E. Bowden et al., Impact of lattice mismatch and stoichiometry on the structure and bandgap of (Fe, Cr)2O3 epitaxial thin films. J. Phys. Condens. Matter Inst. Phys. J. **26**, 251–259 (2014). https://doi.org/10.1088/0953-8984/26/13/135005
26. S.J. Scierka, A. Proctor, M. Houalla et al., Determination of the distribution of chromium oxidation states in reduced Cr/Al 2 O 3 catalysts from XPS by factor analysis and curve fitting. Surf. Interface Anal. **20**, 901–908 (1993). https://doi.org/10.1002/sia.740201105
27. C.Y. Cheng, C.N. Hong, Growth of hydrogen-free diamond-like carbon films by a particle-free hollow-cathode arc ion plating system. Thin Solid Films **498**, 206–211 (2006). https://doi.org/10.1016/j.tsf.2005.07.089
28. N. Paik, Raman and XPS studies of DLC films prepared by a magnetron sputter-type negative ion source. Surf. Coat. Technol. **200**, 2170–2174 (2005). https://doi.org/10.1016/j.surfcoat.2004.08.073
29. K.W.R. Gilkes, H.S. Sands, D.N. Batchelder et al., Direct observation of sp^3 bonding in tetrahedral amorphous carbon using ultraviolet Raman spectroscopy. Appl. Phys. Lett. **70**, 1980–1982 (1997). https://doi.org/10.1016/S0022-3093(98)00190-2
30. A.C. Ferrari, J. Robertson, Interpretation of Raman spectra of disordered and amorphous carbon. Phys. Rev. B: Condens. Matter **61**, 14095–14107 (2000). https://doi.org/10.1103/PhysRevB.61.14095
31. M. Aliofkhazraei, A.S. Rouhaghdam, Fabrication of TiC/WC ultra hard nanocomposite layers by plasma electrolysis and study of its characteristics. Surf. Coat. Technol. **205**, S51–S56 (2010). https://doi.org/10.1016/j.surfcoat.2010.04.010
32. T. Horiuchi, K. Yoshida, M. Kano et al., Evaluation of adhesion and wear resistance of DLC films deposited by various methods. Plasma Process. Polym. **6**, 410–416 (2009). https://doi.org/10.1002/ppap.200930004
33. V. Bellido-González, N. Stefanopoulos, F. Deguilhen, Friction monitored scratch adhesion testing. Surf. Coat. Technol. **74**, 884–889 (1995). https://doi.org/10.1016/0257-8972(95)08315-4
34. C.W.M. Moura e Silva, J.R.T. Branco, A. Cavaleiro, How can H content influence the tribological behaviour of W-containing DLC coatings. Solid State Sci. **11**, 1778–1782 (2009). https://doi.org/10.1016/j.solidstatesciences.2009.01.001
35. A.J. Perry, Scratch adhesion testing of hard coatings. Thin Solid Films **107**, 167–180 (1983). https://doi.org/10.1016/0040-6090(83)90019-6
36. J.X. Liao, Z. Tian, J. Xu et al., The effect of H2/C2H2 ratio on the structure and tribological properties of carbon thin films prepared by PBII. Surf. Coat. Technol. **201**, 2871–2877 (2006). https://doi.org/10.1016/j.surfcoat.2006.05.038